Supporting Information

An Unprecedented Fully Reduced {Mo^{V}_{60}} Polyoxometalate: From All-Inorganic Molecular Light-Absorber Model to Improved Photoelectronic Performance

Xue-Xin Li,§[a] Tuo Ji,§[a] Jun-Yang Gao,§[a] Wei-Chao Chen,*[a] Ye Yuan,[a] Hao-Yan Sha,[b] Roland Faller,[b] Guo-Gang Shan,[a] Kui-Zhan Shao,[a] Xin-Long Wang*[a] and Zhong-Min Su[a]

[a]*Key Laboratory of Polyoxometalate and Reticular Material Chemistry of Ministry of Education, Department of Chemistry, Northeast Normal University Ren Min Street No. 5268 Changchun, Jilin, 130024 P. R. China*

[b]*Department of Chemical Engineering, University of California, Davis, CA 95616, USA*

E-mail: chenwc061@nenu.edu.cn; wangxl824@nenu.edu.cn

§ These authors have contributed equally.

Characterization Methods.

IR spectra were recorded on an Alpha Centauri FTIR spectrophotometer on pressed KBr pellets in the range 400~4000 cm^{-1}. Elemental analyses were analyzed on a Plasma-Spec-II ICP atomic emission spectrometer. Water contents were determined by TG analyses on a PerkinElmer TGA7 instrument in flowing N_2 with a heating rate of 10 °C min^{-1}. UV−vis-NIR spectra were obtained by using a 752 PC UV/Vis spectrophotometer. XRD studies were performed with a Rigaku D/max-IIB X-ray diffractometer at a scanning rate of 1° min^{-1} with $Cu_{K\alpha}$ radiation (λ = 1.5418 Å). Electrospray ionization mass spectrometry was carried out on a Bruker Micro TOF-QII instrument, the solution of the investigated systems were prepared in water. The fluorescence spectra were measured on the Edinburgh FLPS-920 steady-state fluorescence spectrometer. XPS was performed on a ESCALAB 250 spectrometer. The vacuum inside the analysis chamber was maintained at 6.2×10^{-6} Pa during the analysis. The morphology of Mo^{V}_{60}/TiO_2 composite was characterized with SEM (FESEM; XL30, FEG, FEI Company). Energy dispersive X-ray spectroscopy (EDS) was obtained from FEI Quanta 200F microscope. The transmission electron microscopy (TEM) was carried out a JEOL-2100 plus transmission electron microscope. Raman spectra were conducted by a Jobin Yvon confocal laser Raman spectroscopy. The Mott–Schottky spots were carried out at ambient environment using the electrochemical workstation (CHI 760E) in a standard three-electrode system at frequencies of 800, 1000 and 1200 Hz. All electrodes were illuminated from the front side using a 300 W Xe lamp equipped with an AM 1.5 G filter (Model SS150, Zolix) to simulate the solar spectrum. The illumination area of the working electrode was set constant at 0.10 cm^2. The photocurrent-voltage (J-V) and electrochemical impedance spectroscopy (EIS) measurements of the DSSCs were conducted on an electrochemical workstation, applying a DC bias at open circuit voltage and an AC voltage with the amplitude of 10 mV under dark conditions. IPCEs was conducted by a solar cell spectral response system (E0201).

Single-crystal X-ray diffraction: Single-crystal X-ray diffraction data for Mo^{V}_{60} was recorded on a Bruker Apex CCD II area-detector diffractometer with graphite-monochromated $Mo_{K\alpha}$ radiation (λ = 0.71073 Å) at 173(2) K. Absorption corrections were applied using multi-scan technique and performed by using the SADABS program (Sheldrick, G. *SADABS*; ver. 2.10; University of Gottingen: Göttingen, Germany, **2003**). The structure of Mo^{V}_{60} was solved by direct methods and refined on F^2 by full-matrix least squares methods by using the SHELXTL (A.L. Spek, *Acta Cryst.* (**2015**). C71, 9–18) minimization on Olex 2 software package (O.V. Dolomanov, L.J. Bourhis, R. J. Gildea, J. A. K. Howard, H. Puschmann, J. Appl. Crystallogr. 2009, 42, 339–341). CCDC number: 2116971 for Mo^{V}_{60}. During the refinement, all the non-H atoms were refined anisotropically. PLATON software was used for SQUEEZE subroutine for both compounds. About 8 Na^+ cation and 15 water molecules were found from the Fourier maps. However, there are still accessible solvent voids in the crystal structure caculated by SQUEEZE subroutine of PLATON software, indicating that some more cations and solvent molecules should exist in the structure, but cannot be found from the weak residual electron peaks. Based on the TGA curve, bond valence sum calculations, elemental analyses as well as SQUEEZE calculation, another 4 water molecules and 28 H^+ were included into the molecular formula directly.

Table S1. Crystallographic data for Mo^{V}_{60}.

Empirical formula	$H_{66}Mo_{60}Na_8O_{187}$
Formula weight	8998.7
Temperature (K)	173.0 K
Crystal system	Tetragonal
Space group	$I4_1/acd$
a/Å	23.5571(4)
b/Å	23.5571(4)
c/Å	61.035(2)
α(°)	90
β(°)	90
γ(°)	90
V/Å^3	33870.5(17)
ρ_{calc}(g/cm^3)	3478
μ/mm^{-1}	36.392
F(000)	32576.0
θ (°)	8.046 to 127.648
Reflections collected	68939
Independent reflections	6942 [R(int) = 0.0478]
GOF	1.042
Final R indices [I>2sigma(I)]	R_1 = 0.0558, wR_2 = 0.1580
R indices (all data)	R_1 = 0.0606, wR_2 = 0.1628

[a] $R_1 = \Sigma||F_o| - |F_c||/\Sigma|F_o|$, [b] $wR_2 = [\Sigma w(F_o^2 - F_c^2)^2/\Sigma w(F_o^2)^2]^{1/2}$.

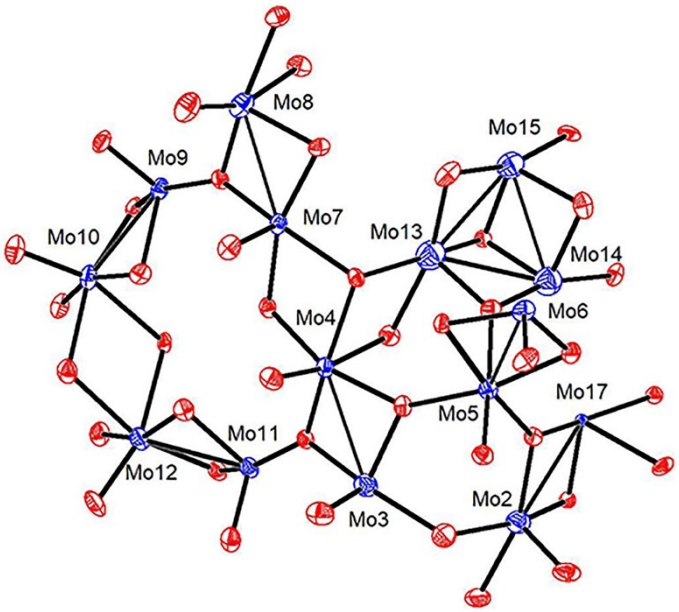

Fig. S1 The asymmetric unit of Mo^{V}_{60}.

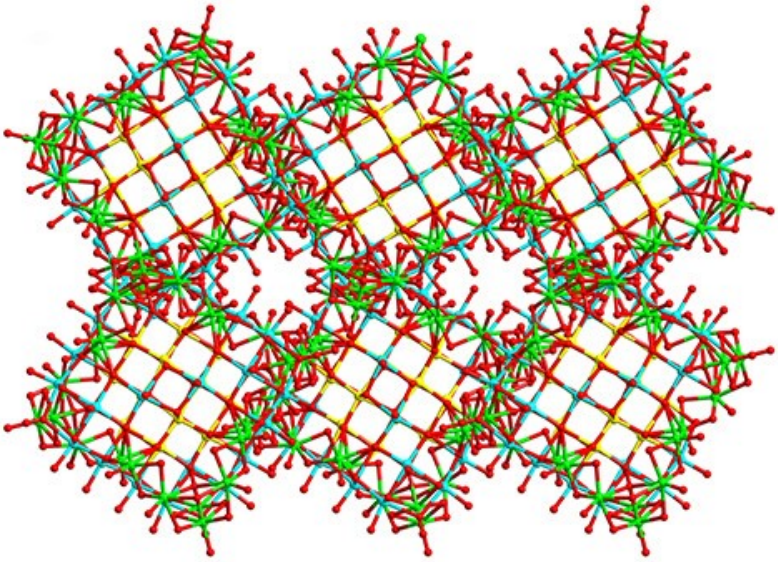

Fig. S2 Packing model of Mo^{V}_{60} along the c-axis.

Table S2. The BVS calculation results of all the protonated oxygen atoms in

Oxygen Code	Bond Valence
O_9	1.260
O_{21}	1.189
O_{22}	1.194
O_{28}	1.297
O_{36}	1.214
O_{40}	1.217
O_{42}	1.219

Table S3. Selected bond lengths (Å) for Mo^{V}_{60}.

Bond	Length (Å)	Bond	Length (Å)	Bond	Length (Å)
Mo(2)-O(9)	2.078(10)	Mo(2)-O(18)	1.994(8)	Mo(2)-O(24)	1.986(8)
Mo(2)-O(28)	2.073(10)	Mo(2)-O(35)	1.682(9)	Mo(2)-O(39)$^{\#2}$	2.129(9)
Mo(3)-O(11)	1.978(8)	Mo(3)-O(16)	1.982(8)	Mo(3)-O(28)	2.080(9)
Mo(3)-O(37)	1.715(9)	Mo(3)-O(39)$^{\#2}$	2.071(9)	Mo(3)-O(40)$^{\#2}$	2.092(9)
Mo(7)-O(4)	2.064(8)	Mo(7)-O(5) $^{\#2}$	2.285(8)	Mo(7)-O(6)	2.080(8)
Mo(7)-O(12)	1.954(8)	Mo(7)-O(13)	1.672(8)	Mo(7)-O(14)	1.951(8)
Mo(8)-O(9)$^{\#3}$	2.097(9)	Mo(8)-O(12)	1.988(9)	Mo(8)-O(14)	1.994(8)
Mo(8)-O(38)	1.676(10)	Mo(8)-O(39)	2.140(9)	Mo(8)-O(40)	2.108(9)
Mo(16)-O(4)	2.137(13)	Mo(16)-O(6)	2.175(13)	Mo(16)-O(8)	1.645(15)
Mo(16)-O(11)	1.914(13)	Mo(16)-O(15)	2.324(15)	Mo(16)-O(16)	1.860(12)
Mo(17)$^{\#1}$-O(2)	1.751(14)	Mo(17)-O(10)	2.101(13)	Mo(17)$^{\#1}$-O(10)	2.091(13)
Mo(17)-O(18)	1.906(13)	Mo(17)-O(23)	2.186(15)	Mo(17)-O(24)	1.909(13)

Symmetry code : $^{\#1}$ -x+1,-y+1/2,z+0.; $^{\#2}$ -y+3/4,x-1/4,-z+1/4; $^{\#3}$ y+1/4,-x+3/4,-z+1/4.

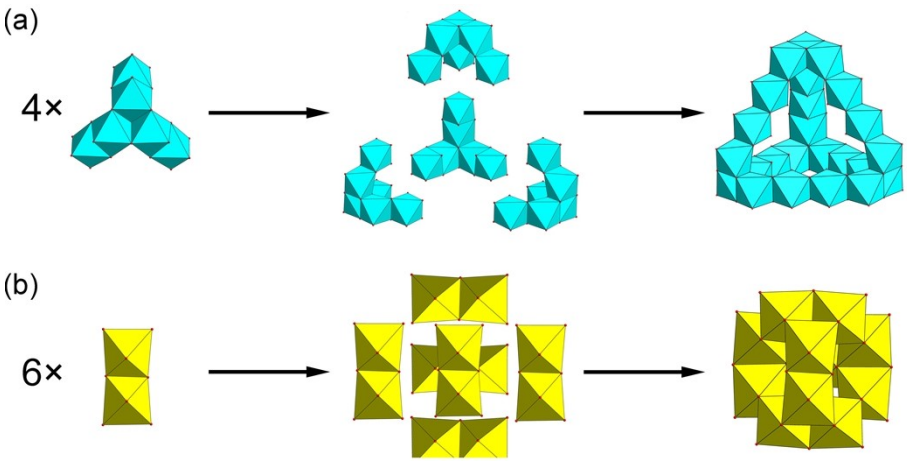

Fig. S3 Polyhedra representations of $\{Mo_{24}\}$ (cyan) and $\{Mo_{12}\}$ (yellow) units with its basic SBBs.

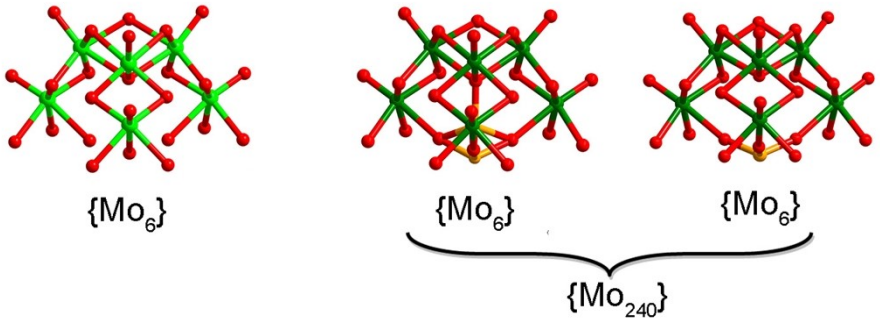

Fig. S4 Ball-and-stick representations of $\{Mo_6\}$ SBBs in Mo^{V}_{60} (left) and Mo_{240} (right). Color code: green, Mo; red, O; orange, S.

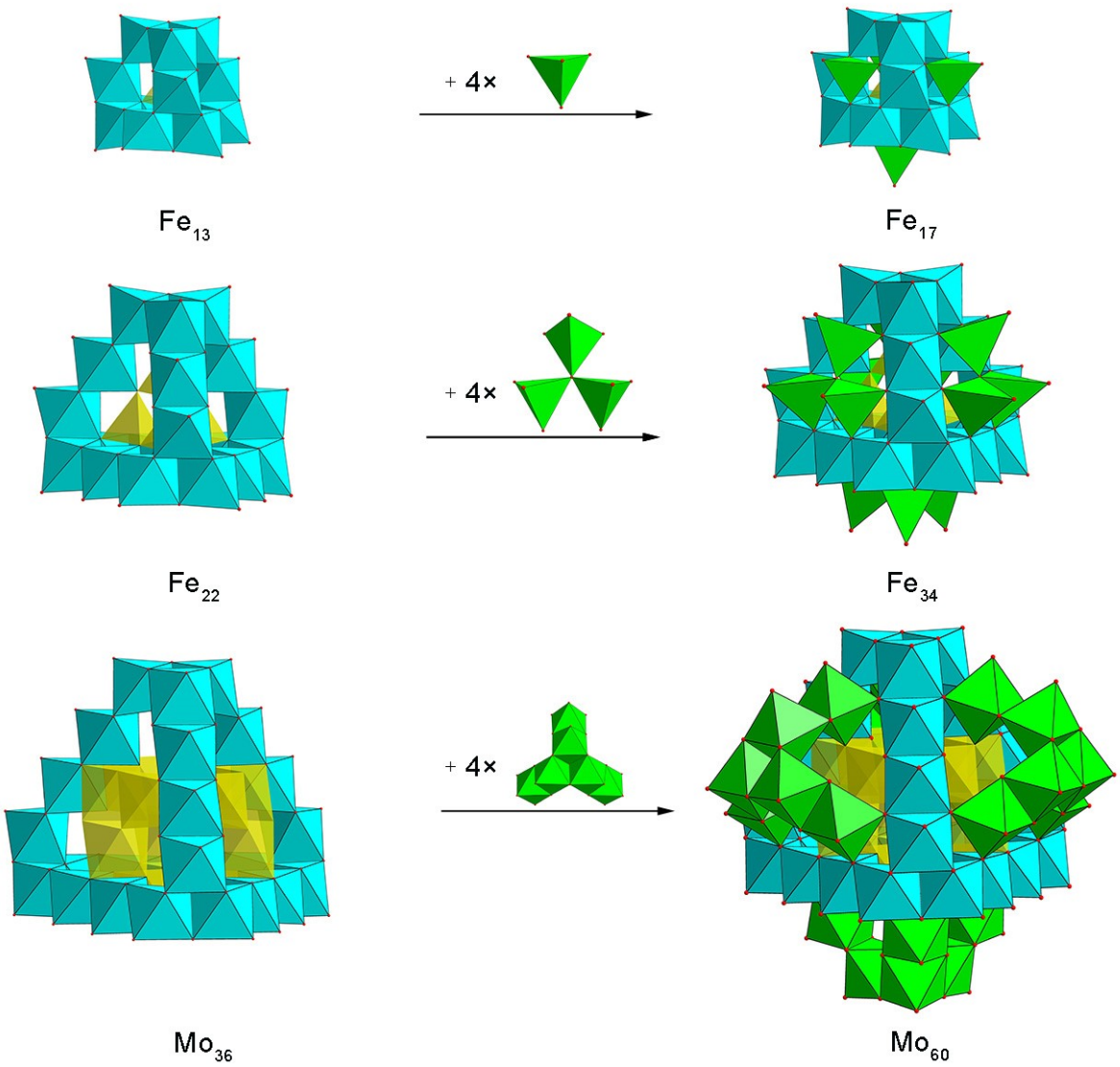

Fig. S5 Polyhedra representations of {Fe_{17}}, {Fe_{34}}, {Mo^{V}_{60}} and its basic SBBs. Color code: green/cyan, Mo; green/cyan/yellow, Fe; red, O.

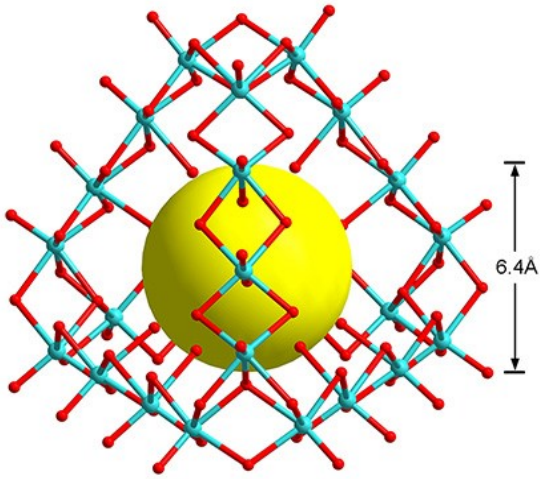

Fig. S6 The inner cavity of {Mo_{24}}. Color code: cyan, Mo; red, O.

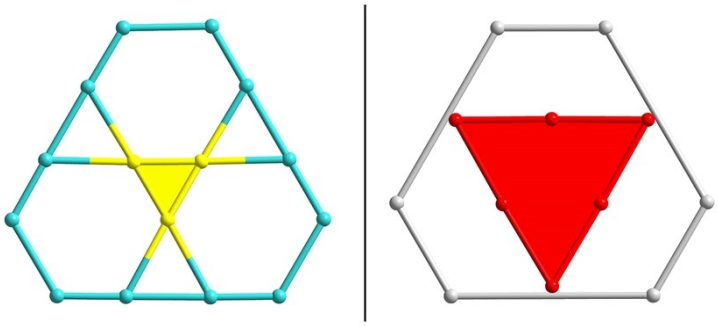

Fig. S7 Metal atom-based skeleton of planar {Mo_{15}} and {Mn_6W_6} in ball-and-stick representation. Color code:blue/yellow, Mo; red, Mn; gray, W.

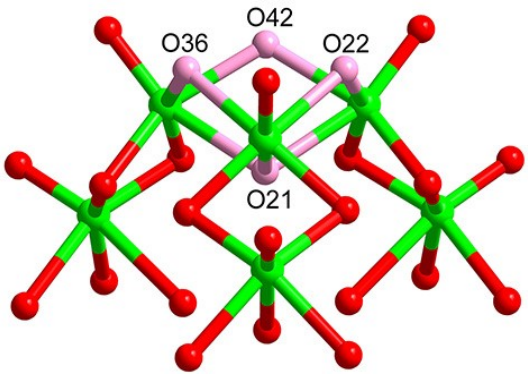

Fig. S8 The protonated oxygen atoms in {Mo_6} SBBs. Color code: green, Mo; red/pink, O.

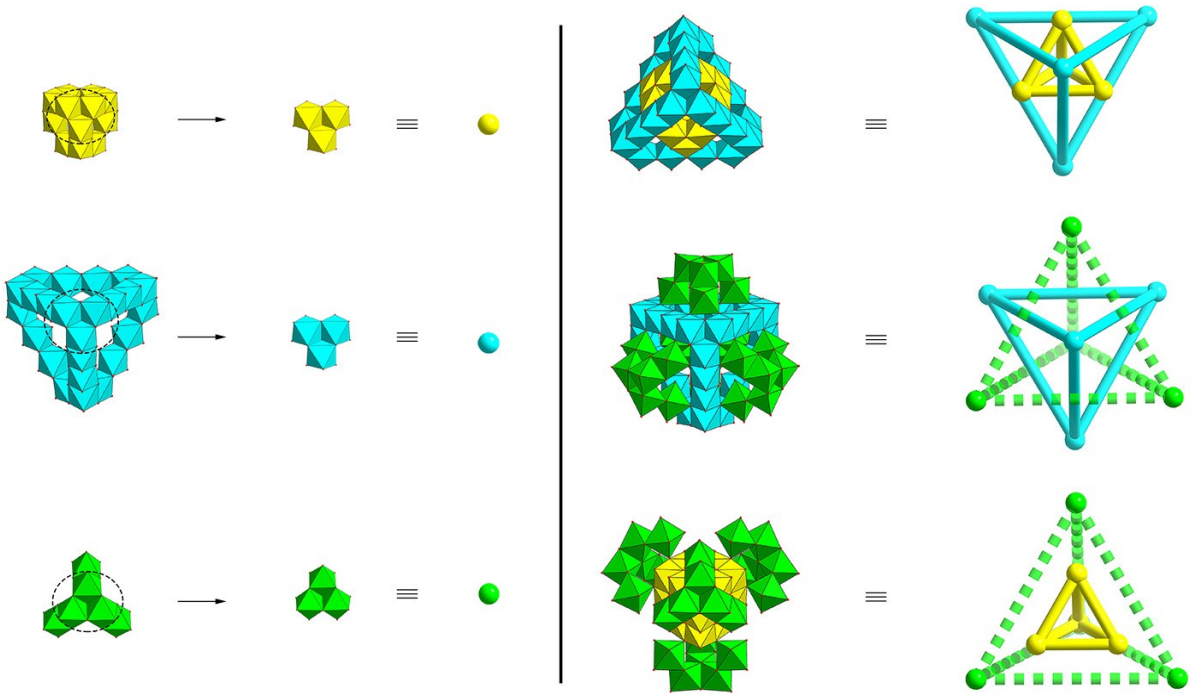

Fig. S9 Polyhedral and ball-and-stick representations of double truncated tetrahedrons quasi-nesting architectures in Mo^{V}_{60}.

Table S4. The BVS calculation results of all the Mo atoms in Mo^{V}_{60}.

Atom	BVS
Mo2	5.386
Mo3	5.327
Mo4	5.352
Mo5	5.254
Mo6	5.416
Mo7	5.430
Mo8	5.305
Mo9	5.394
Mo10	5.335
Mo11	5.304
Mo12	5.223
Mo13	4.519
Mo14	4.545
Mo15	4.556
Mo17	5.332

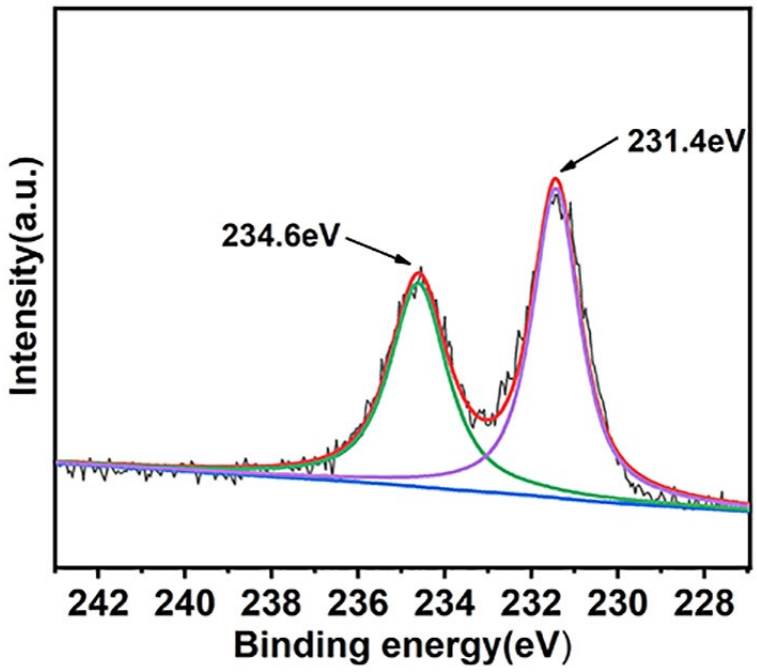

Fig. S10 The XPS spectrum of Mo^{V}_{60}.

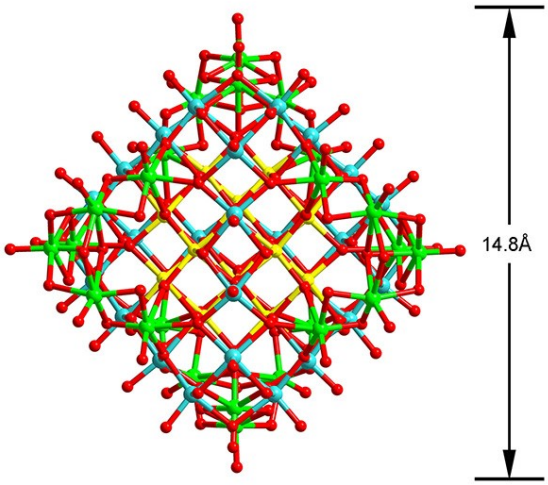

Fig. S11 The outer diameter of Mo^{V}_{60}. Color code: green/yellow/cyan, Mo; red, O.

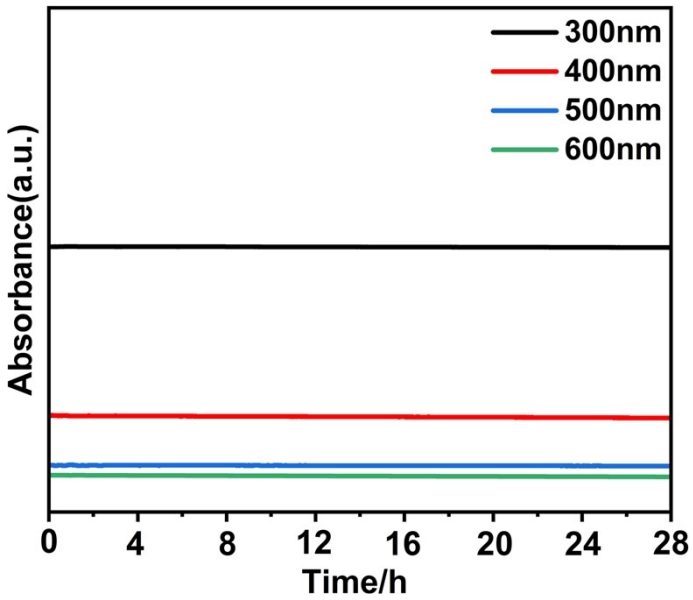

Fig. S12 Changes in UV/Vis spectra of {Mo^{V}_{60}} in water over a 24 h.

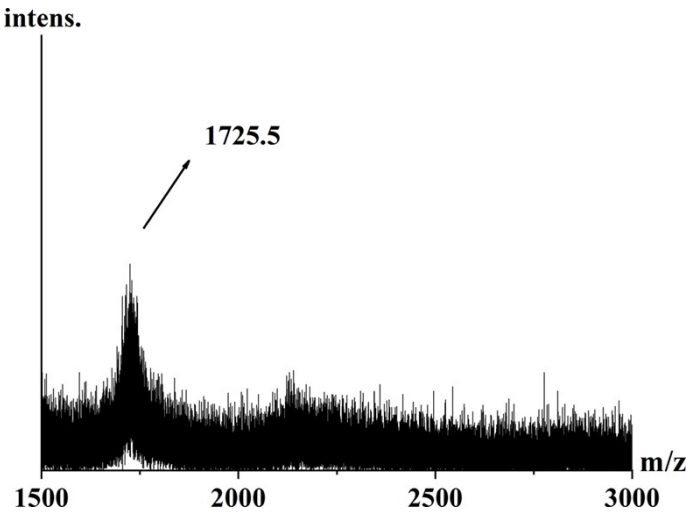

Fig. S13 ESI-MS spectra of Mo^{V}_{60}.

Table S5. Assignment of peaks of Mo^{V}_{60}.

Observed *m/z*	Calculated *m/z*	Charge	Molecular mass	Polyanion
1725.5	1726.3	-5	8631.5	$\{Na_3[Mo^{V}_{60}O_{140}(OH)_{28}](H_2O)_5\}^{5-}$

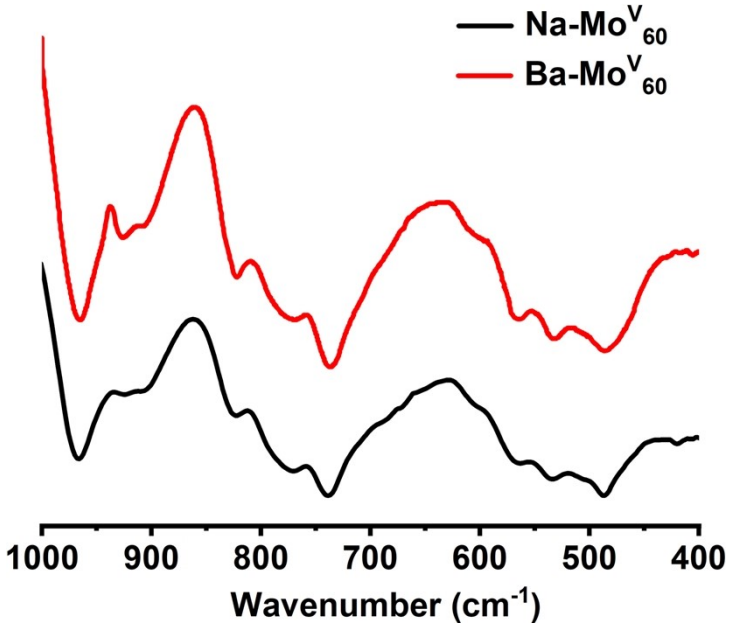

Fig. S14 IR spectra for Na-Mo^{V}_{60} (black) and its cation exchange Ba-Mo^{V}_{60} (red).

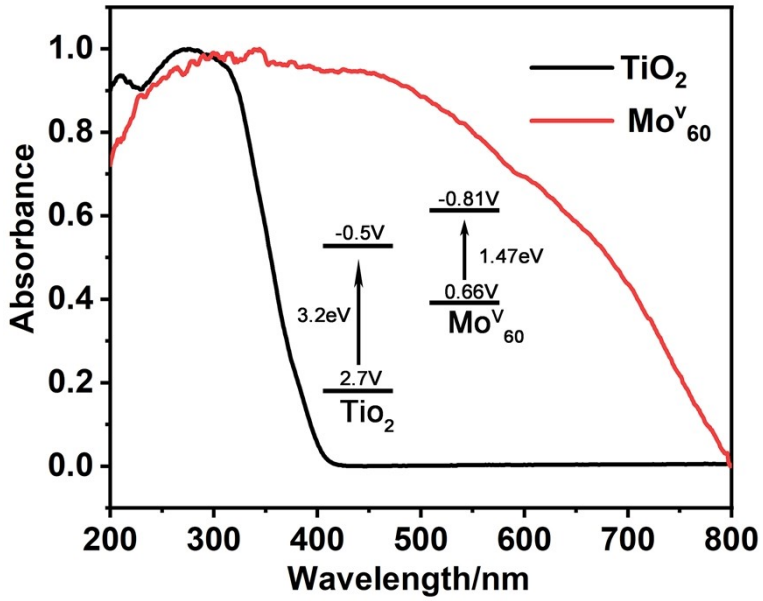

Fig. S15 The UV-vis spectrum of Mo^{V}_{60} (red line)and TiO_2 (black line).

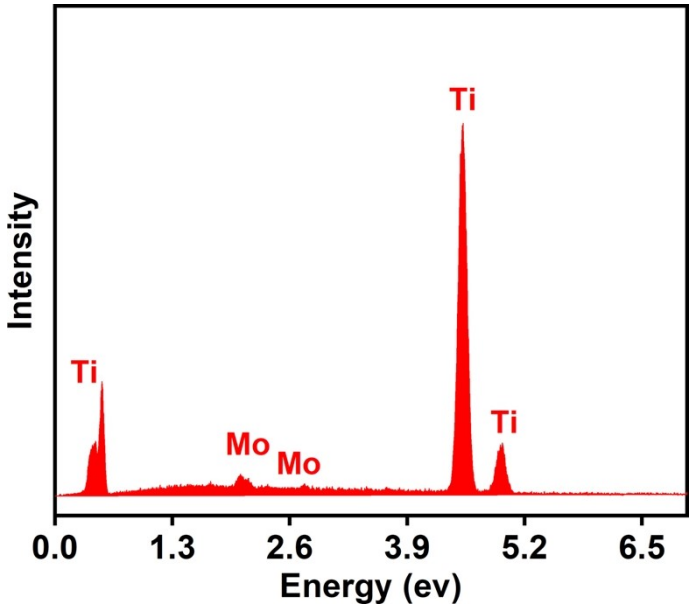

Fig. S16 The EDS spectrum of $Mo_{60}{}^{V}$-TiO_2 composite.

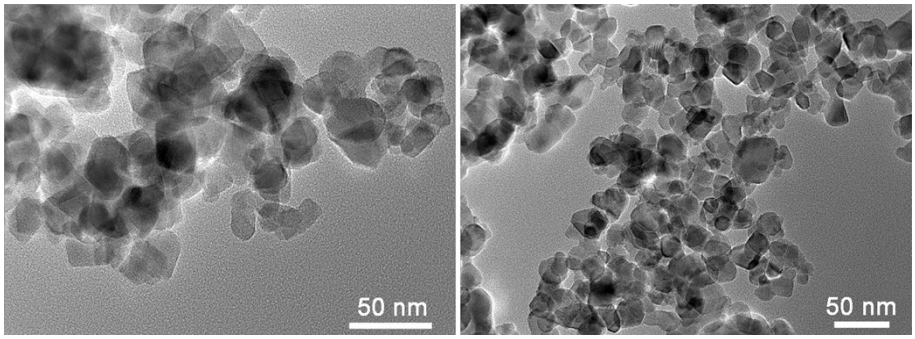

Fig. S17 TEM images of pure P25 TiO_2.

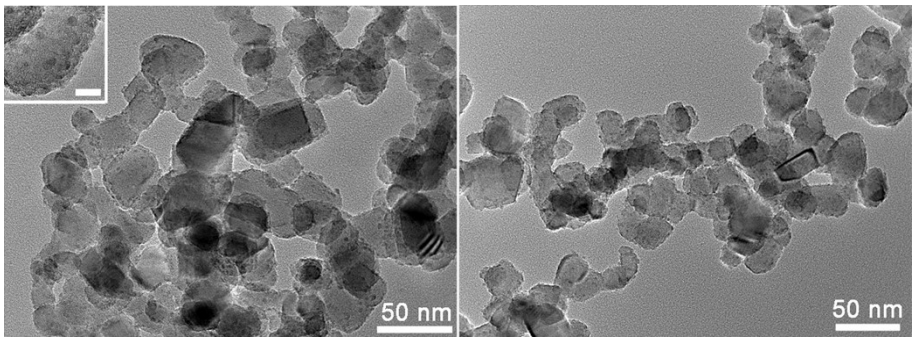

Fig. S18 TEM images of Mo^{V}_{60}/TiO_2 composite. (inset scale bar: 5 nm)

Table S6. A survey of binding energies for typical Mo centers in Mo(IV), Mo(V) and Mo(VI) oxidation states.

	Compounds	Mo state	$3d_{5/2}$	$3d_{3/2}$	*Ref.*
1	nano-MoO_2 catalyst	Mo(IV)	228.8 eV	232.0 eV	*Water Res.*, 2021, 192, 116834
2	MoS_2-Ni/TiO_2		229.0 eV	232.3 eV	*Langmuir*, 2006, 22, 5867-5871
3	$H_{y3}MoO_{3-x4}$		229.1 eV	232.3 eV	*J. Am. Chem. Soc*., 2012, 134, 16178-16187
4	MoS_2/ACF cloth		229.3 eV	232.5 eV	*Nanoscale*, 2014, 6, 5351-5358
5	RGO decorated MoS_2 nanoflowers		229.4 eV	232.6 eV	*ACS Appl. Mater. Interfaces.*, 2015, 7, 12625-12630
6	$K[Co(bpy)_3][Mo(CN)_8]\cdot 8H_2O$	Mo(V)	231.0 eV	234.2 eV	*Inorg. Chem.*, 2010, 49, 2765-2772
7	$[PyPS]_3(NH_4)_3Mo_7O_{24}$		231.0 eV	234.1 eV	*Chem. Eng. J.*, 2019, 358, 419-426
8	Mo oxides in Ni superalloys		231.1 eV	234.3 eV	*J. Alloy.Compd.*, 2022, 895, 162657
9	$[\varepsilon\text{-}PMo^{V}_{8}Mo^{VI}_{4}O_{37}(OH)_3Zn_4](TPB)_{3/2}\cdot 6H_2O$		231.2 eV	234.4 eV	*Angew. Chem. Int. Ed.*, 2019, 58, 16110-16114
10	$EV[Mo_9O_{28}]$ (EV^{2+} = ethyl viologen cation)		231.3 eV	234.7 eV	*Chem. Commun.*, 2018, 54, 14077-14080
11	$Na_8[Mo^{V}_{60}O_{140}(OH)_{28}]\cdot 19H_2O$		231.4 eV	234.6 eV	*this work*
12	MoO_3 after hydrodeoxygenation		231.5 eV	234.6 eV	*Nat. Catal.*, 2018, 1, 960–967
13	Mo-doped $W_{18}O_{49}$ ultrathin nanowires		231.6 eV	234.7 eV	*J. Am. Chem. Soc.*, 2012, 140, 9434–9443
14	Pd/MoO_{3-x}		231.7 eV	234.8 eV	*Adv. Mater.*, 2015, 27, 4616–4621
15	$Na_{15}\{[Mo_{154}O_{462}H_{14}(H_2O)_{70}]_{0.5}[Mo_{152}O_{457}H_{14}(H_2O)_{68}]_{0.5}\}$ca.400$H_2O$		231.9 eV	235.1 eV	*Mater. Today Chem.,* 2020, 16, 100221-100228
16	Commercial MoO_3	Mo(VI)	232.6 eV	235.7 eV	*Angew. Chem. Int. Ed.*, 2014, 53, 2910–2914
17	MoO_3		233.2 eV	236.3 eV	*Adv. Mater.*, 2015, 27, 4616–4621

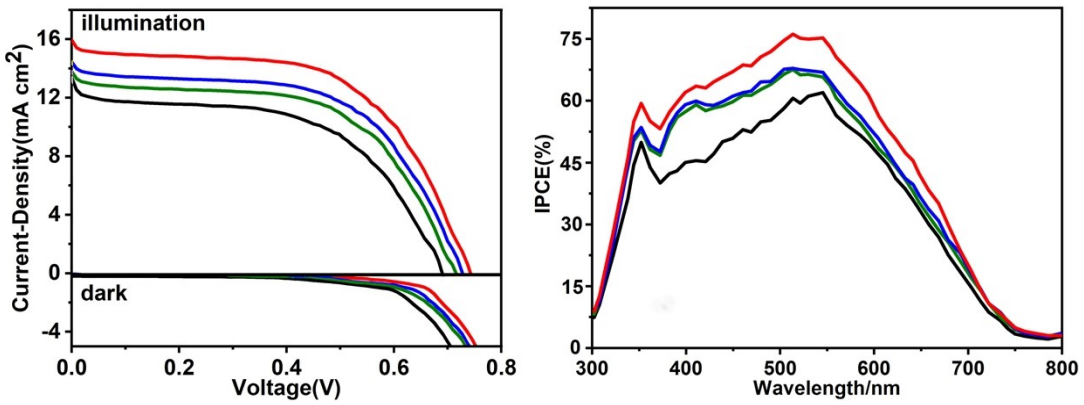

Fig. S19 *J-V* (left) and IPCE (right) curves of the DSSCs with different proportions of Mo^{V}_{60}/N719 and single N719 as the photoanodes. (black: pure N719, red: 5% Mo^{V}_{60}/N719, blue: 3% Mo^{V}_{60}/N719, green: 7% Mo^{V}_{60}/N719)

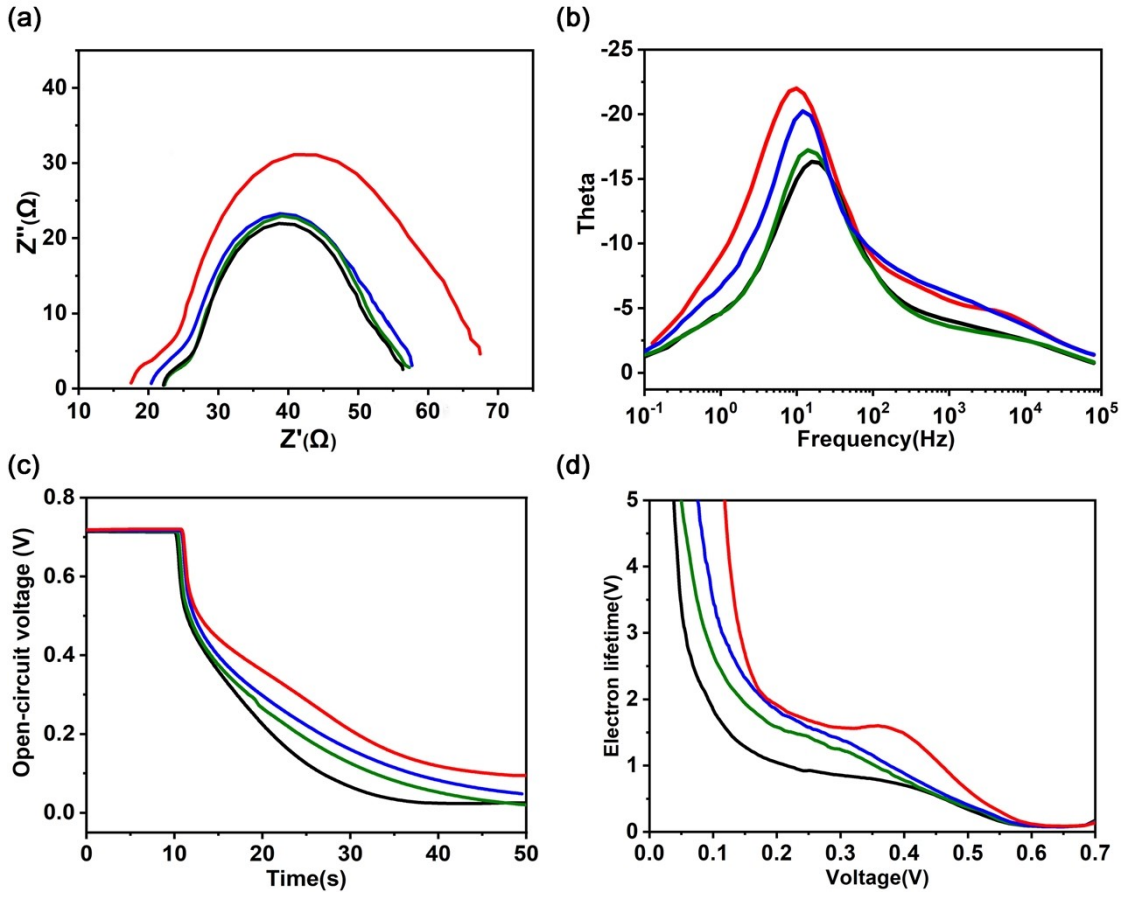

Fig. S20 (a) Nyquist plots. (b) Bode phase plots. (c) OCVD curves of different DSSCs. (d) Electron lifetime calculated from OCVD. (black: pure N719, red: 5% Mo^{V}_{60}/N719, blue: 3% Mo^{V}_{60}/N719, green: 7% Mo^{V}_{60}/N719)

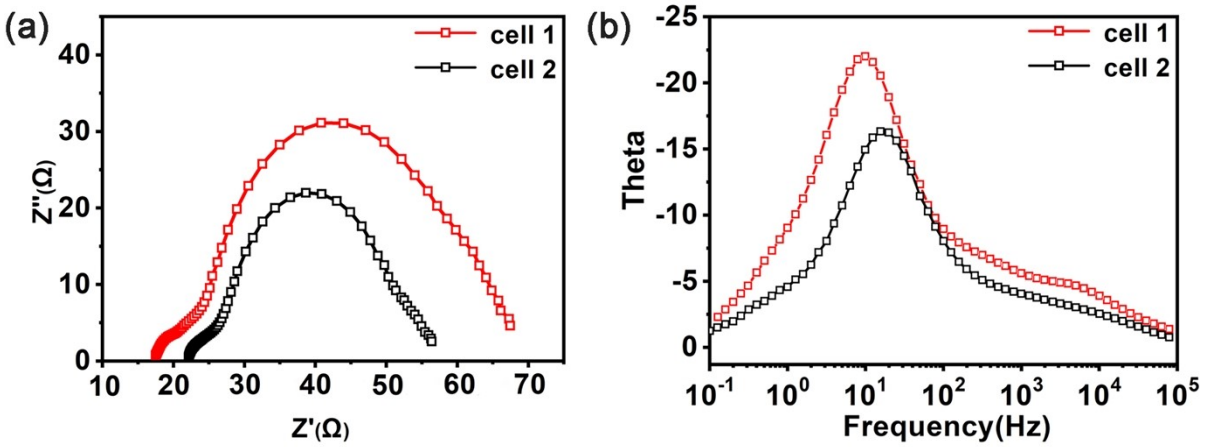

Fig. S21 The EIS spectra of DSSCs based on Mo^{V}_{60}/N719 sensitization: (a) Nyquist plots and (b) Bode phase plots. (cell 1: Mo^{V}_{60}/N719 co-sensitization, cell 2: single N719 sensitization)

Table S7. Photovoltaic parameters of different DSSCs.

Percentage	J_{sc}(mA cm^{-2})	V_{oc}(V)	*FF*(%)	η(%)
0	13.36	0.682	0.569	5.18
3%	14.55	0.716	0.572	5.96
5%	15.94	0.734	0.566	6.63
7%	14.43	0.725	0.569	5.95